

PROCEEDINGS OF SPIE

[SPIDigitalLibrary.org/conference-proceedings-of-spie](https://spiedigitallibrary.org/conference-proceedings-of-spie)

Novel localized surface plasmon resonance based optical fiber sensor

Harald Ian D. I. Muri, Dag Roar Hjelme

Harald Ian D. I. Muri, Dag Roar Hjelme, "Novel localized surface plasmon resonance based optical fiber sensor," Proc. SPIE 9702, Optical Fibers and Sensors for Medical Diagnostics and Treatment Applications XVI, 97020L (7 March 2016); doi: 10.1117/12.2212652

SPIE.

Event: SPIE BiOS, 2016, San Francisco, California, United States

Novel localized surface plasmon resonance based optical fiber sensor

Harald Ian D.I. Muri^a and Dag Roar Hjelme^a

^aNorwegian University of Science and Technology, Gunnerus gate 1, Trondheim, Norway

ABSTRACT

Over the last decade various optical fiber sensing schemes have been proposed based on local surface plasmon resonance (LSPR). LSPR are interacting with the evanescent field from light propagating in the fiber core or by interacting with the light at the fiber end face. Sensor designs utilizing the fiber end face is strongly preferred from a manufacturing point of view. However, the different techniques available to immobilize metallic nanostructures on the fiber end face for LSPR sensing is limited to essentially a monolayer, either by photolithographic structuring of metal film, thermal nucleation of metal film, or by random immobilization of nanoparticles (NP). In this paper, we report on a novel LSPR based optical fiber sensor architecture. The sensor is prepared by immobilizing gold NP's in a hydrogel droplet polymerized on the fiber end face. This design has several advantages over earlier designs. It dramatically increase the number of NP's available for sensing, it offers precise control over the NP density, and the NPs are position in a true 3D aqueous environment. The sensor design is also compatible with low cost manufacturing. The sensor design can measure volumetric changes in a stimuli-responsive hydrogel or measure binding to receptors on the NP surface. It can also be used as a two-parameter sensor by utilizing both effects. We present results from proof-of-concept experiments demonstrating a pH sensor based on LSPR sensing in a poly(acrylamide-co-acrylic acid) hydrogel embedding gold nanoparticles.

Keywords: Fiber optic sensors, smart hydrogel, hydrogel, coupled LSPR, LSPR, nanoplasmonics, pH sensor, proof-of-concept

1. INTRODUCTION

Fiber optic sensors have been proposed in various schemes over the last decade based on local surface plasmon resonance (LSPR).¹⁻⁴ The most common features of LSPR fiber optic sensors are free label sensing, fast response times, high sensitivity and high selectivity. The LSPR fiber optic sensing is often achieved through two schemes: (1) The propagating light in the fiber core that creates an evanescent field is interacting with the LSPR at fiber end face.^{1,2} (2) The propagating light in the fiber core that is interacting with LSPR at the fiber side face.^{3,4} Theoretical and experimental investigations of the interactions between localized and propagating surface plasmons have also been carried out for various applications.⁵ The use of fiber end face as a sensor design offers simpler manufacture methods compared the utilization of the side face since the sensor design is less dependent on the removal of cladding and the steps involved in the surface preparations.

The LSPR is often observed for nanometer-sized metallic structures. The absorption and scattering of incident light on metallic nanostructures depends on the light frequency, size, shape, the dielectric environment, the material composition and the separation between the LSPR in the nanostructure.⁶ Due to the resonant oscillating nature of the conducting electrons in the metallic nanostructure, an enhancement occurs of the absorption and scattering of the incident light for specific frequencies. The spectral properties of noble metal particles can be described by an exact solution well known as the Mie theory for spherical particles.⁷ A geometrical quantity relates the incident light to the scattered, absorbed, or the extinct power,

$$\sigma_{\text{sca}} = \frac{P_{\text{sca}}}{I_{\text{inc}}} = \frac{2\pi}{|k|^2} \sum_{L=1}^{\infty} (2L+1)(|a_L|^2 + |b_L|^2) \quad (1a)$$

Further author information: (Send correspondence to Harald Ian Muri)

Harald Ian Muri: E-mail: harald.i.muri@hist.no, Telephone: +4773412688

Dag Roar Hjelme: E-mail: dag.r.hjelme@hist.no, Telephone: +4773559604

$$\sigma_{\text{ext}} = \frac{P_{\text{ext}}}{I_{\text{inc}}} = \frac{2\pi}{|k|^2} \sum_{L=1}^{\infty} (2L+1) \text{Re}(a_L + b_L) \quad (1b)$$

$$\sigma_{\text{abs}} = \frac{P_{\text{abs}}}{I_{\text{inc}}} = \sigma_{\text{ext}} - \sigma_{\text{sca}} \quad (1c)$$

where L are integers representing dipole for $L=1$ or multipoles for $L > 1$, and k is the incoming wavevector. a_L and b_L are parameters composed of the Riccati-Bessel functions ψ_L and χ_L that are described as

$$a_L = \frac{m\psi_L(mx)\psi_L(x) - \psi_L(mx)\psi_L(x)}{m\psi_L(mx)\chi_L(x) - \psi_L(mx)\chi_L(x)} \quad (2a)$$

$$b_L = \frac{\psi_L(mx)\psi_L(x) - m\psi_L(mx)\psi_L(x)}{\psi_L(mx)\chi_L(x) - m\psi_L(mx)\chi_L(x)} \quad (2b)$$

where $x = k_m r$, r is the radius of the particle, k_m is the wavenumber of the incident light within a medium, $m = \frac{\tilde{n}}{n_m}$, n_m is the real refractive index of the surroundings of metal and $\tilde{n} = n_R + in_I$ is the complex refractive index of the metal. To express a simpler solution to Eq. 1a and 1b, a dipole can be considered for very small particles ($x \ll 1$) following an approximation of the Riccati-Bessel function by Bohren and Huffman.⁸ The extinction and scattering cross-section for nanoparticle (NP) plasmon resonances can then be expressed as,

$$\sigma_{\text{sca}} = \frac{32\pi^4 \varepsilon_m^2 V^2 (\varepsilon_1 - \varepsilon_m)^2 + (\varepsilon_2)^2}{\lambda^4 (\varepsilon_1 + 2\varepsilon_m)^2 + (\varepsilon_2)^2} \quad (3a)$$

$$\sigma_{\text{ext}} = \frac{18\pi \varepsilon_m^{\frac{3}{2}} V \varepsilon_2}{\lambda (\varepsilon_1 + 2\varepsilon_m)^2 + (\varepsilon_2)^2} \quad (3b)$$

where ε_1 and ε_2 are dielectric functions of the complex metal dielectric function $\tilde{\varepsilon}(\lambda) = \varepsilon_1 + i\varepsilon_2$, V is the particle volume, and λ the wavelength of the incident light. Maximum extinction or scattered cross section occurs when the condition of $\varepsilon_1 = -2\varepsilon_m$ is met. This also explains a dependence of the LSPR peak on the surrounding dielectric environment. Mie theory describes also solutions for multipolar localized modes by considering the integers $L > 1$ for spherical particles. For any aspect ratio, the Mie solutions can be extended by using Gans theory in the small particle approximation.⁹

As the theory of LSPR is well established, modelling and computations of fiber optic LSPR sensor designs are feasible as a tool to discover new designs as well new nanoplasmonic effects. The different fiber optic LSPR sensor designs mentioned above have often metallic nanostructures on end face or side face limited to monolayers manufactured by photolithographic structuring of metal film, thermal nucleation of metal film or random immobilization of NP's. This paper reports on the development of a novel LSPR based optic fiber sensor architecture where the sensor is prepared by immobilizing polymerized hydrogel-containing gold nanoparticles (GNP) droplet on the fiber end face. This arrangement's advantages over earlier designs lies in the increase of GNP density available for sensing, the precise control over the GNP density in the hydrogel, having GNP distributed in a 3D aqueous environment, and the low cost manufacturing. The sensing can be a function of the volumetric changes in the hydrogel, receptors on the GNP surface interacting selectively with the analyte, or surface-enhanced Raman scattering (SERS). By using NP's of different size, shape or material composition it can also be used for multiplexed sensing where several effects are measured simultaneously. This design represents a proof-of-concept experiment where the LSPR peak wavelength are measured as a function of volume size of the poly(acrylamide-co-acrylic acid)-GNP hydrogel. Since acrylic acid is a comonomer in the polymer network, the hydrogel volume can be manipulated by adjusting the pH of the solution surrounding the hydrogel. The deprotonation or protonation of acrylic acid results in an influx or outflux of water in the hydrogel, respectively. In this way, the fiber optic LSPR design is also demonstrated as a pH sensor.

2. MATERIALS AND METHODS

2.1 Materials

The gels were prepared by using following chemicals: acrylamide (AAM) (99%, Sigma Aldrich), acrylic acid (AAC) (99%, Sigma Aldrich), N,N-methylenebisacrylamide (BIS) ($\geq 99.5\%$, Sigma Aldrich), 1-hydroxycyclohexyl phenyl ketone (99%, Sigma Aldrich), dimethyl sulfoxide (DMSO) ($\geq 99.9\%$, Sigma Aldrich), octamethylcyclotetrasiloxane (98%, Sigma Aldrich), 3-(trimethoxysilyl) propyl methacrylate (Silane A174) (98%, Sigma Aldrich), citrate stabilized spherical 80nm gold nanoparticles (GNP) ($7.8 \cdot 10^9$ particles/mL, Absorption max: 551-557nm, Sigma Aldrich), phosphate buffered saline (PBS) (Tablet, Sigma Aldrich) and squalane (99%, Sigma Aldrich). MilliQ (mq) water (resistivity 18.2 M/cm, Millipore Simplicity 185) was used for all solutions. Hydrochloric acid (HCL) (1.0M, Sigma Aldrich) and sodium chloride (NaCl) (18%w/V, VWR) were added to mq water to prepare solutions for inducing change in the volume of the hydrogel. GNP solution was heated up to 40 °C under stirring to evaporate away water so a GNP density of $1.95 \cdot 10^{11}$ particles/mL were achieved. AAM, AAC and BIS were dissolved in PBS solution (pH 7.4) to prepare a stock solution with 30 wt% AAM-AAC, molar ratio 15/85 AAM/AAC, and with 2 mol % BIS. A pregel solution with and without GNP were prepared by adding PBS solution (pH 7.4) and densified GNP solution to the AAM-AAC/BIS stock solution, respectively (10 wt% AAM-AAC, and 2 mol % BIS).

2.2 Setup of fiber optic instrument

The fiber optic instrument illustrated in Fig. 1 consist of a tungsten halogen light source (HL-2000-FHSA-LL, Ocean Optics) connected to a $\text{\O}400\mu\text{m}$ multimode (MM) SMA optical patch cable (QP400-2-UV-VIS) that propagate the white light (360-2400 nm) further to the first arm of the $\text{\O}200\mu\text{m}$ 2x2 50/50 MM coupler (50/50, FCMH2-FC, Thorlabs). FC/PC to SMA adapter (ADAFCSMA1, Thorlabs) was used between the $\text{\O}400\mu\text{m}$ SMA optical patch cable and the $\text{\O}200\mu\text{m}$ 2x2 50/50 MM coupler. A coreless termination fiber, $\text{\O}125\mu\text{m}$ cladding was fused to the second arm of the $\text{\O}200\mu\text{m}$ 2x2 50/50 MM coupler with a splicer (Fitel Fusion Splicer, Furukawa Electric) to prevent back reflection of the fiber end face. The third arm of the coupler was fused to the sensor segment 200 μm MM optical fiber (FT200EMT, Thorlabs) with the splicer. The hydrogel was chemically bond to the end face of the sensor segment through silanization described in Sec. 2.3. Further, the fourth arm of the $\text{\O}200\mu\text{m}$ 2x2 50/50 MM coupler was connected to the spectrometer (QE65Pro, Ocean Optics) through a $\text{\O}400\mu\text{m}$ MM SMA optical patch cable with FC/PC to SMA adapter. A program (Spectrasuite, Ocean Optics) was used for reading out the spectrum.

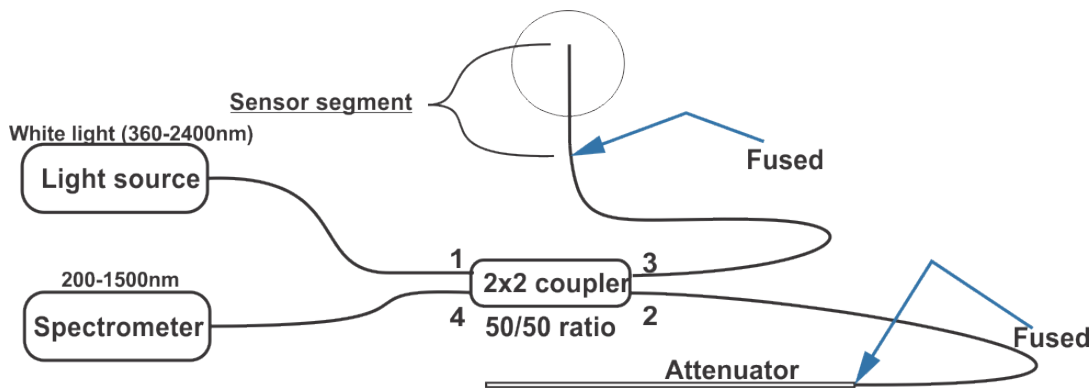


Figure 1: Set up of the fiber optic instrument based on reflection measurements

2.3 Fabrication of fiber optic sensor segment

The sensor segments of $\text{\O}200\mu\text{m}$ MM optical fibers were stripped of the jacket and cleaned with 96% ethanol, cut (Cleaver MS-7310, Melbye Skandinavia) and prepared for silanization.¹⁰ The fibers were soaked in a solution 0.01M HCl for 15 min to activate the surface for silanization, cleaned with mq water and then immersed in

a solution of 3-(trimethoxysilyl) propyl methacrylate (0.084 M, nitrogen purged octamethylcyclotetrasiloxane) for 10 min. The fibers were then cleaned with 96% ethanol and stored for up to two weeks. The pregel solutions from Sec. 2.1 were used further for the synthesis of hydrogel on the silanized fiber end face. 0.01M 1-hydroxycyclohexyl phenyl ketone photoinitiator (PI) in DMSO was added to the pregel solution to a volume ratio of 31/2000 PI/Pregel so a final pregel solution was made. A drop of squalane added with PI (2.7mg/mL) was deposited on a glass rod. The silanized fiber was located in the squalane-PI drop and an aliquot of the final pregel solution was transferred to the end face of the silanized fiber by a pipet (Finnpipette F2, Thermo Scientific). Next, the gel-fiber was aligned with the Ø365 μm Core Multimode Optical Fiber (FG365UEC, Thorlabs) with an optical stage under observation in an optical stereomicroscope (SZX7, Olympus). The Ø365 μm Core Multimode Optical Fiber propagated light from LED at 365nm (M365F1, Thorlabs) that illuminated the gel-fiber and cured it for 10 min. The polymerized gel-fiber was subsequently immersed in pentane to remove impurities for 5s and stored in PBS solution until further use.

2.4 Reflection measurements of GNP embedded in hydrogel

To locate the LSPR spectrum it was necessary to record the reference spectrum of hydrogel without the GNP for each of the solutions containing certain pH and ionic strengths. The dark spectrum was recorded by having the room light and the tungsten halogen light source turned off. The reflection spectra was obtained by using following relations for reflectance,

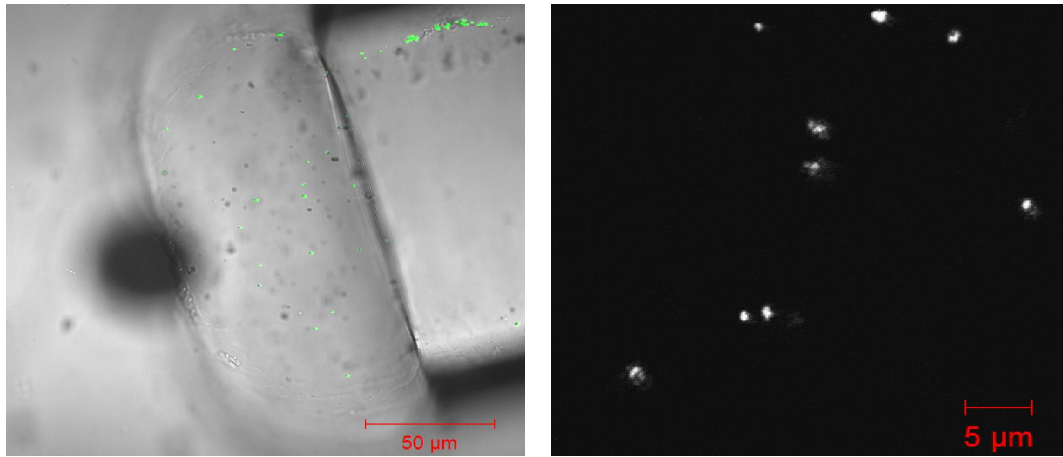
$$I_R = \left(\frac{S_\lambda - D_\lambda}{R_\lambda - D_\lambda} \right) \cdot 100\% \quad (4)$$

where I_R is reflection spectra, S_λ sample spectra, R_λ is reference spectra, and D_λ is the dark spectra. The hydrogel swelling/deswelling with and without GNP was induced by dipping the gel-fiber into pH solutions at 4.1, 3.8, 3.5 and 3.2 for a constant ionic strength (IS) at 0M, 0.274M, 0.822M and, 1.096M. The reference and sample spectra were recorded after the hydrogel swelling/deswelling had reached equilibrium. The hydrogel-fiber was washed in PBS after each measurement until hydrogel equilibrium was reached. The washing in PBS was performed to let the hydrogel undergo only the function of deswelling for each measurement. pH and IS was controlled with pH/IS meter (inoLab pH/ION 7320, WTW), electrode selective towards Cl (Cl 800 (BNC), WTW), pH electrode (pHenomenal MIC 220, VWR Collection), and temperature measurer (pHenomenal TEMP21, VWR Collection). All the experiments were carried out at room temperature and the pH and IS of the solutions were adjusted by adding HCl and NaCl to mq water.

3. RESULTS AND DISCUSSION

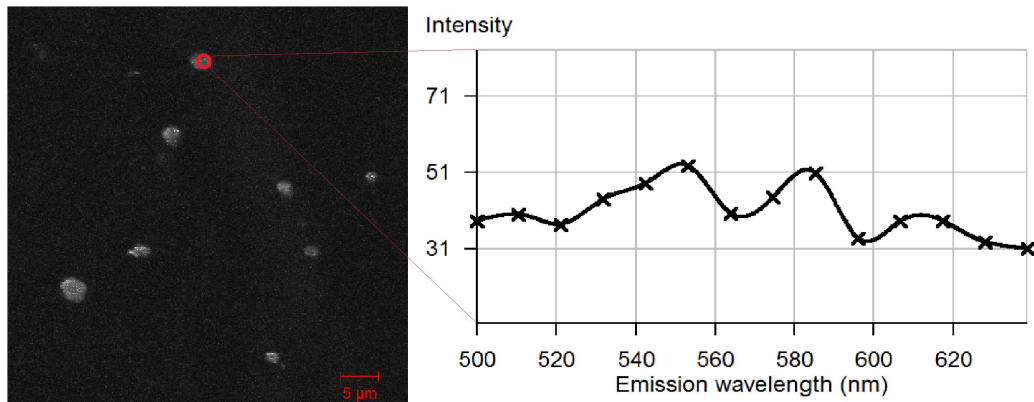
3.1 Sensor fabrication and characterization

Confocal laser scanning microscope (CLSM) images of hydrogel on fiber with GNP are shown in Fig. 2. Transmission and reflection images of hydrogel on fiber with GNP by using incident laser at 543nm are shown in Fig. 2a. Only reflection image of hydrogel on fiber with GNP is shown in Fig. 2b. The green spots in Fig. 2a represents backscattered intensities in the gel-fiber. The grey spots of backscattered intensities from image in Fig. 2b shows to have size between 1-2.5 μm . Grey spots of backscattered intensities are also visible in Fig. 2c were a pulsed TiSp-laser laser (80MHz) at 790nm was used and a spectra measured. The maximum peaks at 555nm, 585nm and 610nm in Fig. 2c may indicate a non-linear response of GNP with a broken centrosymmetry or a clustered influenced photoluminescence of the GNP.^{11,12} Studies have shown that a pulsed laser (80MHz) at 790nm may generate non-linear response from GNP creating multipolar nature of the plasmons or photoluminescence depending on the size shape and the dielectric of the surroundings of the GNP.^{12,13} Densifying the GNP solution may have induced the clustering including following fabrication processes: 1) A smaller negative charge of the citrate groups on the surface as a result of the acidity of the pregel solution may have protonated the citrate groups on the GNP so agglomeration of particles have been induced. 2) The polymerization of the monomers with 10 w% AAM-AAC have been performed by exciting the PI with LED light so free radicals have been released. The free radicals, AAM, AAC, and BIS may have influenced the surface charge of the GNP inducing agglomeration. The densification and clustering of GNP have also redshifted the LSPR from 551-557nm (original GNP solution) to 580nm.



(a) Transmission and reflection image of hydrogel on fiber with GNP with laser at 543nm

(b) Reflection image of hydrogel on fiber with GNP with laser at 543nm



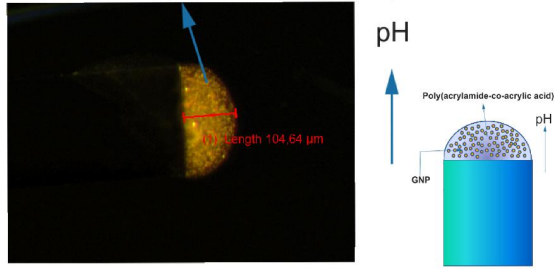
(c) Reflection image of hydrogel with GNP with pulsed laser TiSp-laser (80MHz) at 790nm including measured spectra

Figure 2: Transmission and reflection image of hydrogel on fiber with GNP including measured spectra of a GNP cluster

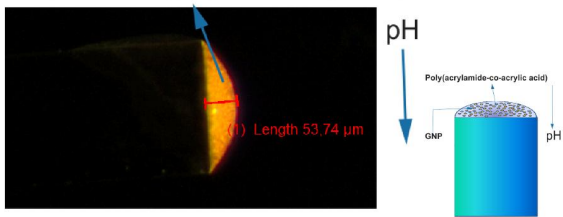
3.2 pH sensing as a function of GNP density

Optical microscope images of GNP embedded in hydrogel are shown in Fig. 3 including an estimation of GNP density in ellipsoid half-volume relative to the original GNP density of $1.95 \cdot 10^{11}$. Fig. 3b shows the increase of GNP density of calculated ellipsoid half-volume illustrated in Fig. 3a as a result of decreasing the pH. The deswelling of hydrogel because of decreasing the pH occurs as the carboxylic group of the acrylic acid is protonated, making acrylic acid no longer negatively charged. Since the polymer network in the hydrogel contain less negative charged molecules, the osmotic pressure of the water-hydrogel interface is reduced resulting in less water contained inside the hydrogel.

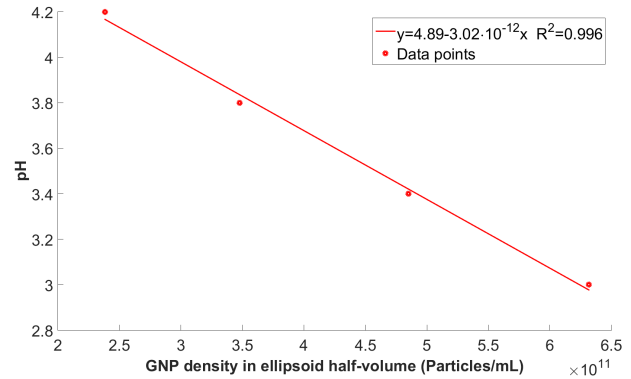
GNP empedded in Poly(acrylamide-co-acrylic acid)



GNP empedded in Poly(acrylamide-co-acrylic acid)



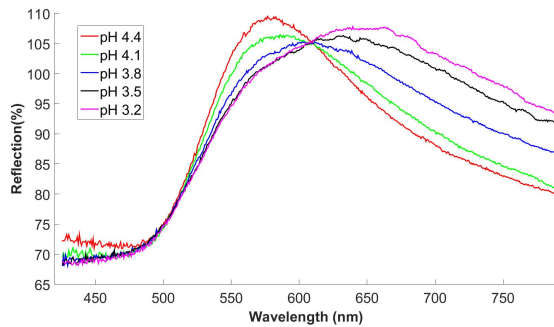
(a) Illustration of the size of hydrogel volume as a function of surrounding pH solution



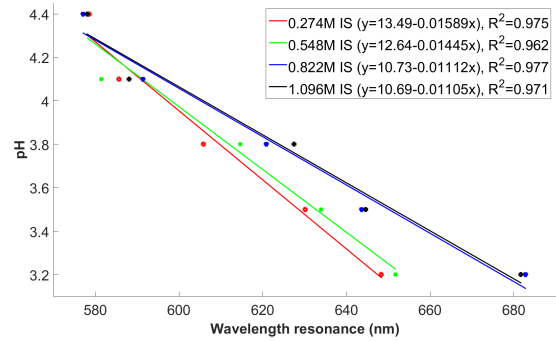
(b) GNP density in hydrogel volume as a function of surrounding pH solution

Figure 3: GNP in hydrogel on fiber in pH solution and linear fit of the GNP density in hydrogel as a function of pH

The linear fit seen in Fig. 3b estimates a measure of the linearity of the GNP density as a function of pH for the following fiber optic LSPR reflection measurements. The LSPR shifts for the hydrogel-GNP deswelling for pH solutions of 4.4-3.2 and IS of 1.096-0.274M are presented in Fig. 4. Fig. 4a shows the LSPR shifts for solutions



(a) Reflection measurements in pH solutions with IS at 0.274M



(b) Linear fit of reflection measurements in pH solutions for constant IS at 0.274, 0.548, 0.822 and 1.096M

Figure 4: Reflection measurements with GNP in hydrogel on fiber in pH solutions for constant IS at 0.274, 0.548, 0.822 and 1.096M

with pH between 4.4-3.2 and constant IS at 0.274M. The LSPR shifts seen in Fig. 4a are typical observations for the fiber optic LSPR probe. The linear fit of the LSPR shifts for pH solutions with constant IS at 0.274, 0.548, 0.822 and 1.096M are shown in Fig. 4b. The LSPR shifts may be induced by two different processes exclusively or combined. As the GNP density in hydrogel is increased for decreased pH, the neighboring distances between GNP will also be decreased. The decrease of neighboring distances between GNP may induce electromagnetic interactions between the localized modes that gives a LSPR redshift observed in Fig. 4. The density of the polymer network are also increasing for a decrease in pH that may change the refractive index around the GNP leading to a shift of the LSPR peak. Control measurements have been carried out by measuring the dependence

of LSPR shift on hydrogel volume size for a decreased GNP density inside the hydrogel. For lower densities of GNP inside the hydrogel, no consistent redshift or blue shift was observed as a function of hydrogel deswelling except small fluctuations of the LSPR peak. This may indicate that the redshift observed in Fig. 4 is a result of the electromagnetic interactions between the localized modes as a function of their interparticle distances. The characteristics of the linear fit in Fig. 4b are shown in Tab. 1. The deviation of the linear fit of the LSPR

Table 1: Characteristics of the linear fit in Fig. 4b

IS	pH at Wavelength resonance=0	$\frac{\Delta\text{pH}}{\Delta\text{Wavelength resonance}}$	R ²
0.274M	13.49	0.01589	0.975
0.548M	12.64	0.01445	0.962
0.822M	10.73	0.01112	0.977
1.096M	10.69	0.01105	0.971

shifting is evident from Tab.1 with $R^2 \approx 0.97$. The R^2 values for the LSPR shifting is also less than the R^2 value shown in Fig. 3b for GNP density as a function of pH. Studies carried out of 50nm GNP in a one-dimensional array suggest that both longitudinal and transverse polarizations of the plasmon polarization depends on the interparticle distance d^{-3} for dipoles.^{14,15} Plasmon polarization of multipolar modes have also a dependence on d^{-4} , d^{-5} ,...for quadrupole, octupole,..., respectively.¹⁶ The studies of red shifting LSPR as a result of densifying GNP have also been carried out theoretically and experimentally.^{17,18} The distribution of LSPR red shifting data in Fig. 4b may be dependent on interparticle distance d^{-3} for dipoles, or the non-uniform distribution of GNP in the hydrogel. The distribution of LSPR red shifting can also be a result of the clustering of GNP as seen in Sec. 3.1 in Fig. 2 as a function of multipolar mode dependence on d^{-3} , d^{-4} , d^{-5} ,... for the plasmon polarization. Considering the hydrogel swelling/deswelling dynamics seen from Fig. 4b, low to high IS at pH 3.2 results in a LSPR change from $\sim 650\text{nm}$ to $\sim 690\text{nm}$, respectively. This may be due to hydrogel swelling/deswelling as a function of the IS. The increase of IS cause either an increase in the protonation of the acrylic acid groups or a decrease in the osmotic pressure at hydrogel-water interface that reduces the hydrogel's ability to contain water.

4. CONCLUSION

Experimental proof-of-concept experiments of GNP embedded in poly(acrylamide-co-acrylic acid) hydrogel on fiber optic end face have been carried out to measure the dependence of LSPR peak wavelength on the hydrogel volume size. The hydrogel volume size was controlled by adjusting the pH of the solution surrounding the hydrogel. Clustered GNP with size of $1\text{-}2.5\mu\text{m}$ have been formed before or during the polymerization of AAM-AAC-GNP pregel solutions. The 3D gold nanostructures forms coupled localized modes as a result of decreasing the interparticle distance between the GNP. The LSPR has a redshift as a function of pH with ratio $\left| \frac{\Delta\text{pH}}{\Delta\text{Wavelength resonance}} \right| \approx 0.012$ and goodness of fit $R^2 \approx 0.97$. In this way, the fiber optic LSPR design is also demonstrated as a pH sensor. The deviation of the linear fit can be a result of the dipole or multipolar mode dependence on d^{-3} , d^{-4} , d^{-5} ,... of the plasmon polarization of the GNP clusters or a non-uniform distribution of the GNP. The LSPR redshifting as a function of pH is also dependent on the IS of the solution resulting in changing the LSPR redshifts to higher wavelengths. The dependence of IS is inherent to the hydrogel itself. As this design is favorable for multiplexed sensing, future work will consist of developing a two or more parameter sensing where the hydrogel volume and the analytes are measured simultaneously. The hydrogel will be selectively sensitive towards a specific biochemical, while the LSPR sensing will be selectively sensitive towards another specific biochemical. Such design can be achieved by measuring the hydrogel volume in the infrared range, while the LSPR is measured on the visible range. The infrared range measurements of hydrogel volume will be based on establishing a Fabry-Perot cavity on the end face of a fiber.¹⁹ Utilizing multiplexing sensing with LSPR in hydrogel volume is also possible by including GNP of different size and shape as well enhancing surface Raman scattering of specific chemicals.

ACKNOWLEDGMENTS

This work was supported in part by the Interreg Sweden-Norway program (IR2015.01) and ENERSENSE (Strategic research program at Norwegian University of Science and Technology-Faculty of Science).

REFERENCES

- [1] Jeong, H.-H., Son, Y.-J., Kang, S.-K., Kim, H.-J., Roh, H.-J., Erdene, N., Park, J.-H., Jeong, D.-H., Lee, H.-Y., and Lee, S.-K., "Fiber-optic refractive index sensor based on the cone-based round structure," *Sensors Journal, IEEE* **13**, 351–358 (Jan 2013).
- [2] Sanders, M., Lin, Y., Wei, J., Bono, T., and Lindquist, R. G., "An enhanced {LSPR} fiber-optic nanoprobe for ultrasensitive detection of protein biomarkers," *Biosensors and Bioelectronics* **61**(0), 95 – 101 (2014).
- [3] Cao, J., Tu, M. H., Sun, T., and Grattan, K. T., "Wavelength-based localized surface plasmon resonance optical fiber biosensor," *Sensors and Actuators B: Chemical* **181**(0), 611 – 619 (2013).
- [4] Srivastava, S. K., Arora, V., Sapra, S., and Gupta, B. D., "Localized surface plasmon resonance-based fiber optic u-shaped biosensor for the detection of blood glucose," *Plasmonics* **7**(2), 261–268 (2011).
- [5] Wang, K., Schonbrun, E., and Crozier, K. B., "Propulsion of gold nanoparticles with surface plasmon polaritons: Evidence of enhanced optical force from near-field coupling between gold particle and gold film," *Nano Lett.* **9**, 2623–2629 (July 2009).
- [6] Mayer, K. M. and Hafner, J. H., "Localized surface plasmon resonance sensors," *Chem. Rev.* **111**, 3828–3857 (June 2011).
- [7] Mie, G., "Beiträge zur optik trüberer medien, speziell kolloidaler metallösungen," *Ann. Physik* **330**(3), 377–442 (1908).
- [8] Bohren, C. F. and Huffman, D., [*Absorption and Scattering of Light by Small Particles*], Wiley (1998).
- [9] Gans, R., "The form of ultramicroscopic gold particles," *Annalen der Physik* **37**, 881–900 (1912).
- [10] Cras, J., Rowe-Taitt, C., Nivens, D., and Ligler, F., "Comparison of chemical cleaning methods of glass in preparation for silanization," *Biosensors and Bioelectronics* **14**(8 - 9), 683 – 688 (1999).
- [11] Butet, J., Bachelier, G., Russier-Antoine, I., Jonin, C., Benichou, E., and Brevet, P.-F., "Interference between selected dipoles and octupoles in the optical second-harmonic generation from spherical gold nanoparticles," *Phys. Rev. Lett.* **105**, 077401 (Aug 2010).
- [12] Beversluis, M. R., Bouhelier, A., and Novotny, L., "Continuum generation from single gold nanostructures through near-field mediated intraband transitions," *Phys. Rev. B* **68**, 115433 (Sep 2003).
- [13] Bachelier, G., Butet, J., Russier-Antoine, I., Jonin, C., Benichou, E., and Brevet, P.-F., "Origin of optical second-harmonic generation in spherical gold nanoparticles: Local surface and nonlocal bulk contributions," *Phys. Rev. B* **82**, 235403 (Dec 2010).
- [14] Maier, S. A., Brongersma, M. L., Kik, P. G., and Atwater, H. A., "Observation of near-field coupling in metal nanoparticle chains using far-field polarization spectroscopy," *Phys. Rev. B* **65**, 193408– (May 2002).
- [15] Maier, S. A., Kik, P. G., and Atwater, H. A., "Observation of coupled plasmon-polariton modes in au nanoparticle chain waveguides of different lengths: Estimation of waveguide loss," *Applied Physics Letters* **81**(9), 1714–1716 (2002).
- [16] Jain, P. K. and El-Sayed, M. A., "Plasmonic coupling in noble metal nanostructures," *Chemical Physics Letters* **487**, 153–164 (Mar. 2010).
- [17] Danckwerts, M. and Novotny, L., "Optical frequency mixing at coupled gold nanoparticles," *Phys. Rev. Lett.* **98**, 026104 (Jan 2007).
- [18] Ghosh, S. K. and Pal, T., "Interparticle coupling effect on the surface plasmon resonance of gold nanoparticles: From theory to applications," *Chem. Rev.* **107**, 4797–4862 (Nov. 2007).
- [19] Tierney, S., Falch, B. M. H., Hjelme, D. R., and Stokke, B. T., "Determination of glucose levels using a functionalized hydrogel optical fiber biosensor: Toward continuous monitoring of blood glucose in vivo," *Anal. Chem.* **81**, 3630–3636 (May 2009).